International Journal of Wavelets, Multiresolution and Information Processing

Signal Analysis and Performance Evaluation of a Vehicle Crash Test with a Fixed Safety Barrier Based on Haar Wavelets

Hamid Reza Karimi*and Kjell G. Robbersmyr
Department of Engineering, Faculty of Engineering and Science, University of Agder
N-4898 Grimstad, Norway
hamid.r.karimi@uia.no; kjell.g.robbersmyr@uia.no

Received 3 November 2009
Revised 20 March 2010

This paper deals with the wavelet-based performance analysis of the safety barrier for use in a full-scale test. The test involves a vehicle, a Ford Fiesta, which strikes the safety barrier at a prescribed angle and speed. The vehicle speed before the collision was measured. Vehicle accelerations in three directions at the centre of gravity were measured during the collision. The yaw rate was measured with a gyro meter. Using normal speed and high-speed video cameras, the behavior of the safety barrier and the test vehicle during the collision was recorded. Based upon the results obtained, the tested safety barrier, has proved to satisfy the requirements for an impact severity level. By taking into account the Haar wavelets, the property of integral operational matrix is utilized to find an algebraic representation form for calculate of wavelet coefficients of acceleration signals. It is shown that Haar wavelets can construct the acceleration signals well.

Keywords: Wavelet; Traffic safety; Safety barrier; Collision; Acceptance criteria.

AMS Subject Classification: 42C40, 35G20, 65M70

1. Introduction

Restraint systems are safety devices that are designed to assist in restraining the occupant in the seating position, and help reduce the risk of occupant contact with the vehicle interior, thus helping reduce the risk of injury in a vehicular crash event. In todays quest for continued improvement in automotive safety, various restraint systems have been developed to provide occupant protection in a wide variety of crash environments under different directions and conditions. It is extremely difficult to present rigorous mathematical treatments to cover occupant kinematics in complicated real world situations [5,40].

Occupant safety during a crash is an important consideration in the design of automobiles. The crash performance of an automobile largely depends on the ability of its structure to absorb the kinetic energy and to maintain the integrity

*Corresponding author. Tel: +47-3723-3259; Fax: +47-3723-3001; E-mail: hamid.r.karimi@uia.no

of the occupant compartment. To verify the crash performance of automobiles, extensive testing as well as analysis are needed during the early stages of design. Various types of full car and component level tests are performed to ensure the structural performance of an automobile during an accident. Two full car tests required by the U.S. National Highway Traffic Safety Administration (NHTSA) are the frontal impact and side impact. In the frontal impact test, the test vehicle hits a rigid wall and the injury is measured in terms of accelerations at various locations (such as head, chest, etc.), using dummies as human surrogates. The occupant protection can be improved by designing the front end in structure to minimize deceleration of the occupant while maintaining the structural integrity of the occupant compartment. In the test procedure for a side impact, a stationary vehicle is struck by a specially designed barrier called an MDB (moving deformable barrier). Two devices representing occupants (SIDs or side impact dummies) are located in the front and rear seat of the struck side of the vehicle. The injury is measured in terms of the peak accelerations of a SID's chest and pelvis. The injury protection for the occupant can be improved by making the car structure stiffer while making the car interior that comes into contact with the occupant softer[13].

In the last ten years, emphasis on the use of analytical tools in design and crash performance has increased as a result of the rising cost of building prototypes and the shortening of product development cycles. Currently, lumped parameter modeling (LPM) and finite element modeling (FEM) are the most popular analytical tools in modeling the crash performance of an automobile[2,6]. The use of lumped parameter modeling in crash-worthiness began in the aerospace industry and was gradually extended to the auto industry. The first successful lumped parameter model for the frontal crash of an automobile was developed by Kamal[20]. From then on this technique was extensively used throughout the auto industry for various car models. In a typical lumped parameter model, used for a frontal crash, the vehicle can be represented as a combination of masses, springs and dampers. The dynamic relationships among the lumped parameters are established using Newton's laws of motion and then the set of differential equations are solved using numerical integration techniques. The major advantage of this technique is the simplicity of modeling and the low demand on computer resources. The problem with this method is obtaining the values for the lumped parameters, e.g. mass, stiffness, and damping. The current approach is to crush the structural components using a static crusher to get force deflection characteristics. The mass is lumped based on the experience and judgment of the analyst. However, because of improper boundary conditions during the component test, it has been observed in many cases that the crush mode for a particular component during the static component crush is quite different from that seen in a full car test. Usually complicated fixtures and additional parts are attached to the component being tested to achieve the proper end conditions. This adds complexity and cost to the component crush test. Since the early 60s, the finite element method (FEM) has been used extensively for linear stress, deflection and vibration analysis. However, its use in crashworthiness analysis

was very limited until a few years ago. The availability of general purpose crash simulation codes like DYNA3D and PAMCRASH, an increased understanding of the plasticity behavior of sheet metal, and increased availability of the computer resources have increased the use of finite element technique in crash simulation during the last few years[16,21,32,38]. The major advantage of an FEM model is its capability to represent geometrical and material details of the structure. The major disadvantage of FE models is cost and time. To obtain good correlation of an FEM stimulation with test measurements, extensive representation of the major mechanisms in the crash event is required. This increases costs and the time required for modeling and analysis.

On the other hand, in recent years, wavelet transform as a new technique for time domain simulations based on the time-frequency localization, or multiresolution property, has been developed into a more and more complete system. This transform found great success in practical engineering problems, such as signal processing, pattern recognition and computational graphics[14,18,35]. Recently, some of the attempts are made in solving surface integral equations, improving the finite difference time domain method, solving linear differential equations and nonlinear partial differential equations and modeling nonlinear semiconductor devices. Several articles have been published recently in the fields of applied mathematics and physics that present wavelet based methods for resolution of (partial differential equations) PDEs[1,4]. These are classified as collocation methods or Galerkin methods[3,7,10,15,17,19,22,23,24,25,26,27,28,29,30,31,37]. The approximation of general continuous functions by wavelets is very useful for system modeling and identification. In recent years, the analytical study of adaptive nonlinear control systems using universal function approximators has received much attention. Recently, the paper Onchis and Suarez Sanchez[34] studied the spectral decomposition and the adaptive analysis of data coming from car crash simulations. The mathematical ingredient of the proposed signal processing technique is the flexible Gabor-wavelet transform or the α-transform that reliably detects both high and low frequency components of such complicated short-time signals. We go from the functional treatment of this wavelet-type transform to its numerical implementation and we show how it can be used as an improved tool for spectral investigations compared to the short-time Fourier transform or the classical wavelet transform.

The present work intends to, emphasizing the advantages of wavelets, analyze performance of the safety barrier for use in a full-scale test. Also in this article, we use the Haar wavelets to calculate wavelet coefficients. The test involves a vehicle, a Ford Fiesta, which strikes the safety barrier at a prescribed angle and speed. The vehicle speed before the collision was measured. Vehicle accelerations in three directions at the centre of gravity were measured during the collision. The yaw rate was measured with a gyro meter. Using normal speed and high-speed video cameras, the behavior of the safety barrier and the test vehicle during the collision was recorded. Based upon the results obtained, the tested safety barrier, has proved to satisfy the requirements for an impact severity level. By taking into account the

Haar wavelets, the property of integral operational matrix is utilized to find an algebraic representation form for calculate of wavelet coefficients of acceleration signals. It is shown that Haar wavelets can construct the acceleration signals well.

This paper is organized as follows. Section 2 describes the wavelet properties. Vehicle kinematics in a fixed barrier impact, including the vehicle dimensions and position of the center of gravity, are summarize in Section 3. Instrumentation during the test is given in Section 4. Section 5 proposes wavelet-based analysis of the measured signals. Finally, Section 6 summarizes the paper.

2. Orthogonal families of Wavelets

Wavelets are a relatively new mathematical concept, introduced at the end of the 1980s[11,12,33]. The term "wavelet" is used in general to describe a function that features compact support. This means that the function is located spatially, only being different from zero in a finite interval.

The great advantage of this type of function, compared to the conventional functions used in data representation, is that different resolution levels can be used to describe distinct space or time regions. This feature is quite useful in signal, sound, and image compression algorithms. When a data set goes through a wavelet transformation, it is decomposed into two types of coefficients: one represents general features (scaling function coefficients) and another describes localized features (wavelet coefficients). In order to perform data compression, the wavelet coefficients corresponding to regions in space of less importance are partially rejected. Then, when the function is reconstructed, high resolution is maintained only in the relevant regions. This localized resolution feature does not exist in plane waves, which have constant resolution throughout the entire domain.

Two functions, the mother scaling function, ϕ , and the mother wavelet, ψ , characterize each orthogonal family. These are defined by the following recursive relations

$$\phi(x) = \sqrt{2} \sum_{j=-m}^{m} h_j \phi(2x - j), \psi(x) = \sqrt{2} \sum_{j=-m}^{m} g_j \phi(2x - j). \tag{2.1}$$

where h_j and g_j are the filters that characterize the family of degree m . These filters must satisfy orthogonality and symmetry relations. Due to the choice of the filters h_j and g_j , the dilations and translations of the mother scaling function, $\phi_k^j(x)$, and the mother wavelet, $\psi_k^j(x)$, form an orthogonal basis of $L^2(\mathbb{R})$. This property has an important consequence: any continuous function, $f(x)$ can be uniquely projected in this orthogonal basis and expressed as, for example, a linear combination of functions ψ_k^j .

$$f(x) = \sum_{j \in \mathbb{Z}} \sum_{k \in \mathbb{Z}} d_k^j \psi_k^j(x) \,. \tag{2.2}$$

where $d_k^j = \int_{-\infty}^{\infty} f(x) \psi_k^j(x) dx$.

2.1. *Expansion of a continuous function*

Regarding to multiresolution analysis, the expansion of a continuous function in wavelet theory can be performed according to two representations. The first scaling function representation involves only the scaling functions; the second, wavelet representation, involves both wavelets and scaling functions. The representations are equivalent and need the exact same number of coefficients. One can move from one representation to the other by using a process designated as wavelet transform[39]. The scaling function representation is given by

$$f(x) = \sum_{k=0}^{2^{J_{max}}} s_k^{J_{max}} \phi_k^{J_{max}}(x)\,. \tag{2.3}$$

where $s_k^{J_{max}} = \int f(x)\phi_k^{J_{max}}(x)dx$ is the scaling function coefficient, J_{max} is the maximum resolution level, and k represents the spatial location. The wavelet representation is given by

$$f(x) = \sum_{k=0}^{2^{J_{min}}} s_k^{J_{min}} \phi_k^{J_{min}}(x) + \sum_{j=J_{min}}^{J_{max}-1} \sum_{k=0}^{2^j} d_k^j \psi_k^j(x)\,. \tag{2.4}$$

where d is the wavelet coefficient and J_{min} is the minimum resolution level,

$$d_k^j = \int_{-\infty}^{\infty} f(x)\psi_k^j(x)dx, \quad s_k^{J_{min}} = \int_{-\infty}^{\infty} f(x)\phi_k^j(x)dx. \tag{2.5}$$

Integrations have to be performed in order to compute the expansion coefficients. Several methods have been proposed in the literature for accomplishing this, starting from a function's discrete values. These methods necessarily introduce a certain approximation error and increase the complexity of the problem, namely in the solution of PDEs. There is, however, a wavelet family for which these integrations are exact: the interpolating wavelets.

2.2. *Haar Wavelet*

The oldest and most basic of the wavelet systems is named *Haar wavelets*[28] which is a group of square waves with magnitudes of ± 1 in certain intervals and zero elsewhere,in other words,

$$\psi(t) = \begin{cases} 1 & \text{if } 0 \le t < \frac{1}{2}, \\ -1 & \text{if } \frac{1}{2} \le t < 1, \\ 0 & \text{otherwise} \end{cases} \tag{2.6}$$

The normalized scaling function is also defined as $\phi(t) = 1$ for $0 \le t < 1$ and zero elsewhere. Just these zeros make the Haar transform faster than other square functions such as Walsh function[9]. We can easily see that the $\phi(.)$ and $\psi(.)$ are compactly supported, they give a local description, at different scales j, of the considered function.

The wavelet series representation of the one-dimensional function $y(t)$ in terms of an orthonormal basis in the interval $[0, 1)$ is given by

$$y(t) = \sum_{i=0}^{\infty} a_i \, \psi_i(t) \tag{2.7}$$

where $\psi_i(t) = \psi(2^j t - k)$ for $i \geq 1$ and we write $i = 2^j + k$ for $j \geq 0$ and $0 \leq k < 2^j$ and also defined $\psi_0(t) = \phi(t)$. Since it is not realistic to use an infinite number of wavelets to represent the function $y(t)$, (2.7) will be terminated at finite terms and we consider the following wavelet representation $\hat{y}(t)$ of the function $y(t)$:

$$\hat{y}(t) = \sum_{i=0}^{m-1} a_i \, \psi_i(t) := a^T \Psi_m(t), \tag{2.8}$$

where $a := \begin{bmatrix} a_0 \; a_1 \; \dots \; a_{m-1} \end{bmatrix}^T$ and $\Psi_m(t) := [\psi_0(t) \, \psi_1(t) \; \dots \; \psi_{m-1}(t)]^T$ for $m = 2^j$ and the Haar coefficients a_i are determined as

$$a_i = 2^j \int_0^1 y(t) \, \psi_i(t) \, dt. \tag{2.9}$$

The approximation error $\Xi_y(m) := y(t) - \hat{y}(t)$ depends on the resolution m. For example, at resolution scale $j = 3$, the eight Haar functions can be represented as

$$H_8 = \begin{bmatrix} \psi_0(t) \\ \psi_1(t) \\ \psi_2(t) \\ \psi_3(t) \\ \psi_4(t) \\ \psi_5(t) \\ \psi_6(t) \\ \psi_7(t) \end{bmatrix} = \begin{bmatrix} 1 & 1 & 1 & 1 & 1 & 1 & 1 & 1 \\ 1 & 1 & 1 & 1 & -1 & -1 & -1 & -1 \\ 1 & 1 & -1 & -1 & 0 & 0 & 0 & 0 \\ 0 & 0 & 0 & 0 & 1 & 1 & -1 & -1 \\ 1 & -1 & 0 & 0 & 0 & 0 & 0 & 0 \\ 0 & 0 & 1 & -1 & 0 & 0 & 0 & 0 \\ 0 & 0 & 0 & 0 & 1 & -1 & 0 & 0 \\ 0 & 0 & 0 & 0 & 0 & 0 & 1 & -1 \end{bmatrix}, \tag{2.10}$$

where the eight columns of the matrix represent the values of $\psi_i(t)$ within the eight time intervals. In (2.10) the number of rows denotes the order of the Haar function. Generally, the matrix H_m can be represented as

$$H_m := \begin{bmatrix} \Psi_m(t_0) \; \Psi_m(t_1) \; \dots \; \Psi_m(t_{m-1}) \end{bmatrix}, \tag{2.11}$$

where $\frac{i}{m} \leq t_i < \frac{i+1}{m}$ and using (2.8), we get

$$\begin{bmatrix} \hat{y}(t_0) \; \hat{y}(t_1) \; \dots \; \hat{y}(t_{m-1}) \end{bmatrix} = a^T H_m. \tag{2.12}$$

For further information see the references[8,28,29,30].

2.3. *Integral Operation Matrix*

In the wavelet analysis of dynamical systems, we consider a continuous operator $\tilde{O}$ on the $L_2(\Re)$, then the corresponding discretized operator in the wavelet domain at resolution m is defined as[28]

$$\tilde{O}^m = T_m \, \tilde{O} T_m \tag{2.13}$$

where T_m is the projection operator on a wavelet basis of proposed resolution. Hence to apply $\tilde{O}^m$ to a function $y(t)$ means that the result is an approximation (in the multiresolution meaning) of $\tilde{O}\,y(t)$ and it holds that

$$\lim_{m\to\infty} \|\tilde{O}^m y - \tilde{O}\,y\|_2 = 0, \tag{2.14}$$

where the operator $\tilde{O}^m$ can be represented by a matrix P_m.

In this paper, the operator $\tilde{O}$ is considered as integration, so the corresponding matrix $P_m =< \int_0^t \Psi_m(\tau)\,d\tau, \Psi_m(t) >= \int_0^1 \int_0^t \Psi_m(\tau)\,d\tau\,\Psi_m^T(t)\,dt$ represents the integral operator for wavelets on the interval at the resolution m. Hence the wavelet integral operational matrix P_m is obtained by

$$\int_0^t \Psi_m(\tau)\,d\tau = P_m \Psi_m(t). \tag{2.15}$$

For Haar function (2.6), the square matrix P_m satisfies the following recursive formula[8,28,29,30]:

$$P_m = \frac{1}{2m}\begin{bmatrix} 2mP_{\frac{m}{2}} & -H_{\frac{m}{2}} \\ H^{-1}_{\frac{m}{2}} & 0 \end{bmatrix} \tag{2.16}$$

with $P_1 = \frac{1}{2}$ and $H_m^{-1} = \frac{1}{m}H_m^T\,diagonal(\mathbf{r})$ where H_m defined in (2.11) and $\mathbf{r} := (1,1,2,2,4,4,4,4,\ldots,\underbrace{(\frac{m}{2}),(\frac{m}{2}),\ldots,(\frac{m}{2})}_{(\frac{m}{2})elements})^T$ for $m > 2$.

3. Vehicle kinematics in a fixed barrier impact

The first and second integrals of the vehicle deceleration, $a(t)$, are shown below. The initial velocity and initial displacements of the vehicle are v_0 and x_0, respectively.

$$a = \frac{dv}{dt},\ \ dv = a\,dt,\ \ \int_{v_0}^{v} dv = \int_0^t a\,dt,\ \ v = v_0 + \int_0^t a\,dt \tag{3.1}$$

$$x = x_0 + \int_0^t \left(v_0 + \int_0^t a\,dt\right)\,dt, \tag{3.2}$$

In the fixed barrier test, vehicle speed is reduced (velocity decreases) by the structural collapse, therefore, the vehicle experiences a deceleration in the forward direction. To study the effect of vehicle deceleration on occupant-restraint performance in a real test, the performance of the safety barrier was determined by performing a full-scale test at Lista Airport[36]. The test involves a vehicle, a Ford Fiesta, which strikes the safety barrier at a prescribed angle and speed. The vehicle speed before the collision was measured. Vehicle accelerations in three directions at the centre of gravity were measured during the collisison. The yaw rate was measured with a gyro meter. Using normal speed and high-speed video cameras, the behaviour of the safety barrier and the test vehicle during the collision was recorded.

3.1. *Vehicle dimensions*

Figure 1 shows the characteristic parameters of the vehicle, and these parameters are listed in Table 1.

Table 1. Vehicle dimensions in [m].

Width	Length	Height	Wheel track	Wheel base	Frontal overhang	Rear overhang
1.58	3.56	1.36	1.42	2.28	0.63	0.65

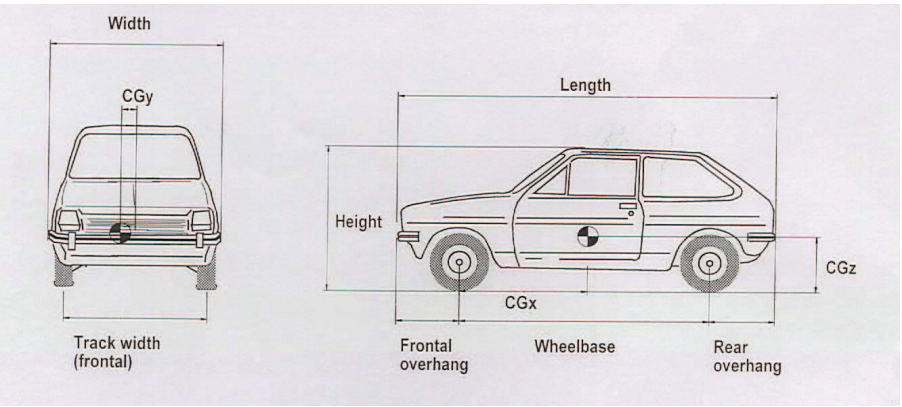

Fig. 1. Vehicle dimensions.

3.2. *The position of the center of gravity*

To determine the position of the center of gravity each test vehicle was first weighed in a horizontal position using 4 load cells. Then the vehicle was tilted by lifting the front of the vehicle. In both positions the following parameters were recorded:

- m_1 : wheel load, front left
- m_2: wheel load, front right

- m_3 : wheel load, rear left
- m_4 : wheel load, rear right
- m_v : total load
- θ : tilted angle
- l : wheel base
- d : distance across the median plane between the vertical slings from the lift brackets at the wheel centers and the load cells.

The horizontal distance between the center of gravity and the front axle centerline, i.e. Longitudinal location, is defined as follows:

$$CG_X = (\frac{m_3 + m_4}{m_v})l$$

and Laterally location is the horizontal distance between the longitudinal median plane of the vehicle and the center of gravity (positive to the left) which is defined as

$$CG_Y = (\frac{m_1 + m_3 - (m_2 + m_4)}{m_v})\frac{d}{2}$$

Also, location of the center of gravity above a plane through the wheel centers is

$$CG_Z = (\frac{m_1 + m_2 - m_f)}{m_v\, tan\theta})l$$

where

- m_f : front mass in tilted position
- m_b : rear mass in tilted position

Table 2. shows the measured parameters to calculate the center of gravity. The position of the centre of gravity for the test vehicle is measured and the result is listed in Table 3.

Table 2. Measured parameters.

m_1 [kg]	m_2 [kg]	m_3 [kg]	m_4 [kg]	m_v [kg]	m_f [kg]	m_b [kg]	d [m]	l [m]	θ [deg]
235	245	182	157	819	443	376	1.71	2.28	22.7

Table 3. The position of the centre of gravity.

Longitudinal location $CG_X[m]$	Lateral location $CG_Y[m]$	Height $CG_Z[m]$
0.94	0.02	0.50

4. Instrumentation

During the test, the following data should be determined:

- Acceleration in three directions during and after the impact
- Velocity 6 m before the impact point

The damage should be visualized by means of:

- Still pictures
- High speed video film

The observations should establish the base for a performance evaluation. Eight video cameras were used for documentation purposes. These cameras are placed relative to the test item as shown in Figure 1. Two 3-D accelerometers were mounted on a steel bracket close to the vehicles centre of gravity. This bracket is fastened by screws to the vehicle chassis. The accelerometer from which the measurements are recorded is a piezoresistive triaxial sensor with accelerometer range: $\pm 1500g$. The yaw rate was measured with a gyro instrument with which it is possible to record $1^o/msec$. Figures 2-4 show the measurements of the 3-D accelerometer in $x-$,$y-$ and $z-$ directions.

Data from the sensors was fed to an eight channel data logger. The logger has a sampling rate of 10 kHz. The memory is able to store 6,5 sec of data per channel. The impact velocity of the test vehicle was measured with an equipment using two infrared beams. The equipment is produced by Alge Timing and is using Timer S4 and photo cell RL S1c. On the test vehicle a plate with a vertical egde was mounted on the left side of the front bumper. This vertical egde will cut the reflected infrared beams in the timing equipment and thereby give signals for calculation of the speed.

The test vehicle was steered using a guide bolt which followed a guide track in the concrete runway. About $7m$ before the test vehicle hit the test item the guide bolt was released. Vehicle accelerations at the centre of gravity was measured, and also the yaw rate of the vehicle. These measurements make it possible to calculate the Acceleration Severity Index (ASI), the Theoretical Head Impact Velocity (THIV), the Post-impact Head Deceleration (PHD) value and the yaw rate. The impact speed of the test vehicle was determined. The ASI-, the THIV- and the PHD-values are calculated according to EN 1317-1 clause 6 and clause 7, and the results are shown in Table 4. Using normal speed- and high-speed video cameras, the behavior of the safety barrier and test vehicle during the collision was recorded, see Figures 5-6. The value of ASI corresponds to the requirement for impact severity level B. The THIV- and PHD-values are below the limiting values.

5. Wavelet-Based Signal Analysis

This section attempts to show the effectiveness of the wavelet technique to represent the measured signals of the test. By choosing the resolution level j = 7 (or $m = 2^8$) and expansion of the acceleration signal $x(t), v(t), a(t)$ in (3.1)-(3.2) by Haar

Table 4. The calculation results.

ASI	THIV	PHD
1.28	29.9	7.8

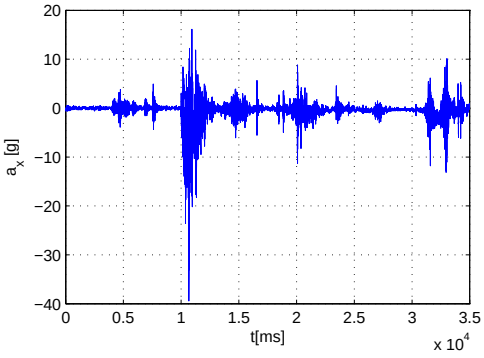

Fig. 2. Acceleration signal in x- direction.

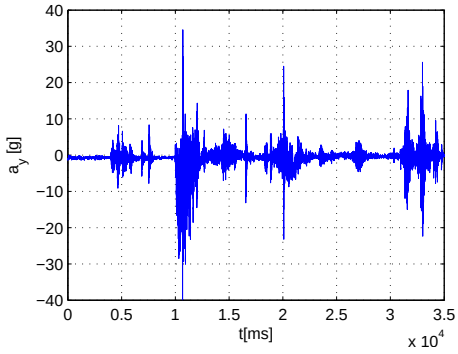

Fig. 3. Acceleration signal in y- direction.

wavelets, we have $x(t) = X\Psi_m(t), v(t) = V\Psi_m(t)$ and $a(t) = A\Psi_m(t)$, in which the row vectors $X, V, A \in \Re^{1\times m}$ are the Haar wavelet coefficient vectors. Utilizing the property of the Haar integral operation matrix, Haar wavelet representation of equations (3.1)-(3.2) are, respectively,

$$V\Psi_m(t) = V_0\Psi_m(t) + \int_0^t A\Psi_m(\tau)\,d\tau = V_0\Psi_m(t) + AP_m\Psi_m(t) \qquad (5.1)$$

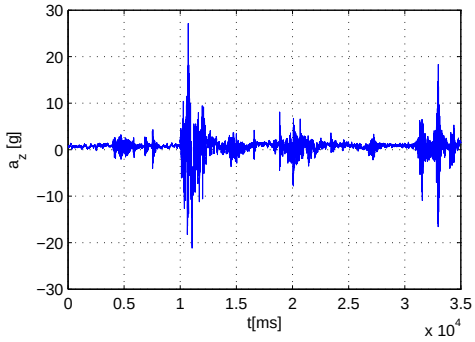

Fig. 4. Acceleration signal in z- direction.

Fig. 5. The situation recorded at the first contact.

and

$$X\Psi_m(t) = X_0\Psi_m(t) + \int_0^t V_0\Psi_m(\tau)d\tau + \int_0^t\int_0^t A\Psi_m(\tau)\,d\tau\,dt,$$
$$= X_0\Psi_m(t) + V_0P_m\Psi_m(t) + AP_m^2\Psi_m(t) \quad (5.2)$$

Constituting the Haar wavelet properties in (5.1)-(5.2), a seven-level wavelet decomposition of the measured x-acceleration signal (a_x) is performed and the results, i.e. the approximation signal (a_7) and the detail signals (d_1-d_7) at the resolution level 7, are depicted in Figures 7-14. One advantage of using these multilevel decomposition is that we can zoom in easily on any part of the signals and examine it in greater detail. Using the approximation signal (a_1) and the detail signal (d_1) at the resolution level 1 by Haar wavelets, Figure 15 compares the constructed signal $a_x(t)$ (solid line) with the real signal (dashed line). It is noted that the approximation error between those curves in Figure 15 is decreasing when the resolution level j

Fig. 6. The situation recorded 0.148 sec after the impact.

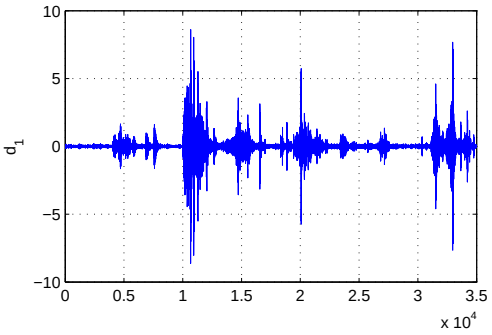

Fig. 7. Detail d_1 of the 7-level Haar wavelet decomposition.

increases. The results in Figures 7-15 show the capability of the Haar wavelets to reconstruct the measured signals well.

6. Conclusions

This paper studied the wavelet-based performance analysis of the safety barrier for use in a full-scale test. The test involves a vehicle, a Ford Fiesta, which strikes the safety barrier at a prescribed angle and speed. The vehicle speed before the collision was measured. Vehicle accelerations in three directions at the centre of gravity were measured during the collision. The yaw rate was measured with a gyro meter. Using normal speed and high-speed video cameras, the behavior of the safety barrier and the test vehicle during the collision was recorded. Based upon the results obtained, the tested safety barrier, has proved to satisfy the requirements for an impact severity level. By taking into account the Haar wavelets, the property

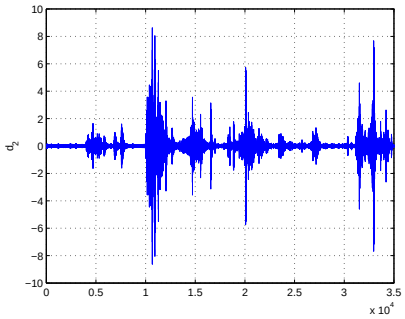

Fig. 8. Detail d_2 of the 7-level Haar wavelet decomposition.

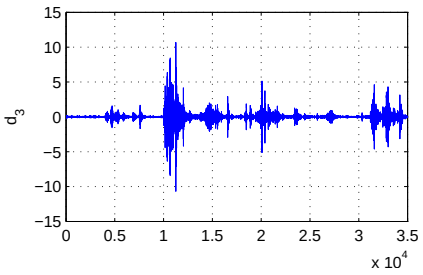

Fig. 9. Detail d_3 of the 7-level Haar wavelet decomposition.

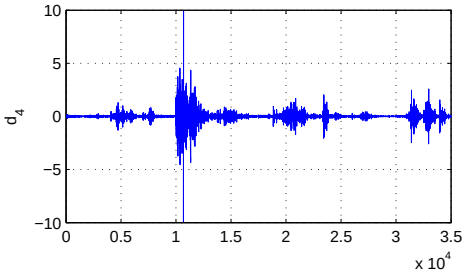

Fig. 10. Detail d_4 of the 7-level Haar wavelet decomposition.

of integral operational matrix was utilized to find an algebraic representation form for calculate of wavelet coefficients of acceleration signals. It was shown that Haar wavelets can construct the acceleration signals well. Future work will investigate the vehicle crash systems by considering nonlinear terms in the model or using other wavelet functions rather than Haar functions.

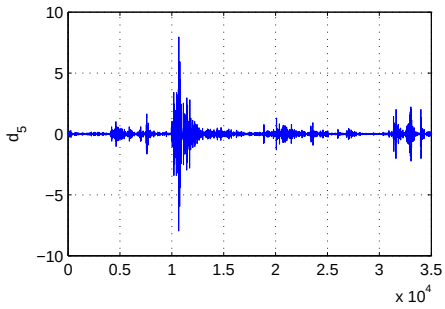

Fig. 11. Detail d_5 of the 7-level Haar wavelet decomposition.

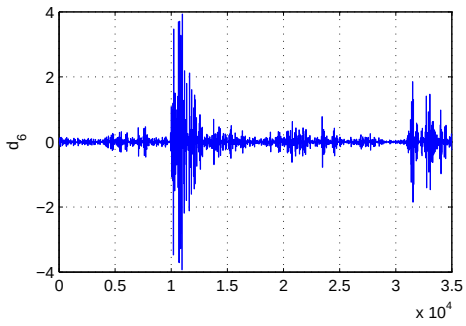

Fig. 12. Detail d_6 of the 7-level Haar wavelet decomposition.

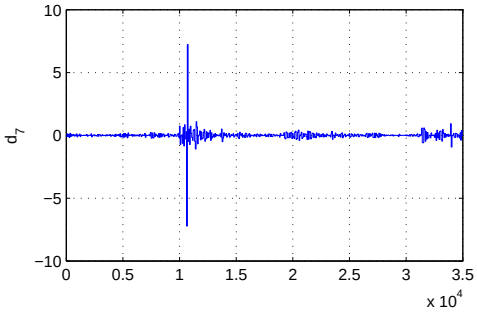

Fig. 13. Detail d_7 of the 7-level Haar wavelet decomposition.

References

1. E. Bacry, S. Mallat, and G. Papanicolaou, A wavelet based space-time adaptive numerical method for partial differential equations, *RAIRO Model. Math. Anal.* **26** (1992)

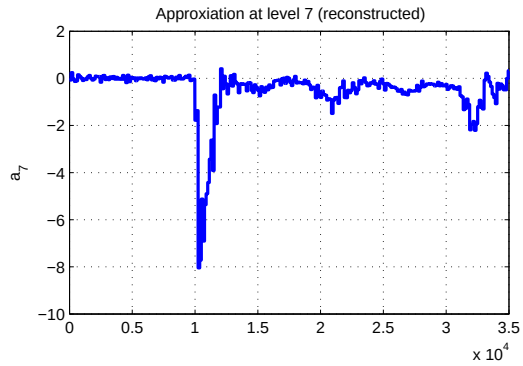

Fig. 14. The approximation signal a_7 of the Haar wavelet decomposition at the resolution level 7.

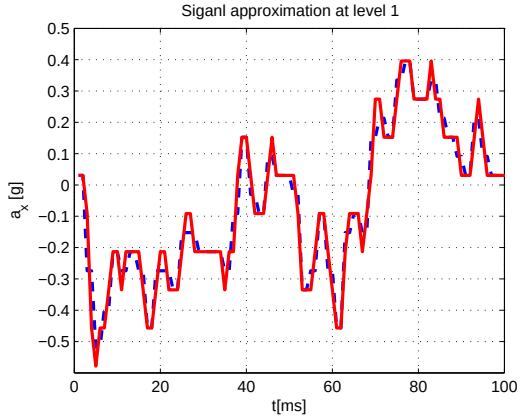

Fig. 15. The constructed signal $a_x(t)$ (solid line) at the resolution level 1 with the real signal (dashed line).

793-834.

2. T. Belytschko, On computational methods for crashworthiness, *Computers and Structure* **42** (1992) 271-279.
3. S. Bertoluzza, Adaptive wavelet collocation method for the solution of Burgers equation, *Transp. Theory Stat. Phys.*, **25** (1996) 339-352.
4. G. Beylkin, and J. Keiser, On the Adaptative numerical solution of nonlinear partial differential equations in wavelets bases, *J. Comput. Phys.*, **132** (1997) 233-259.
5. P.D. Bois, C.C. Chou, B.B. Fileta, T.B. Khalil, A.I. King, H.F. Mahmood, H.J. Mertz and J. Wismans, *Vehicle crashworthiness and occupant protection*, American Iron and Steel Institute, 2004.
6. M. Borovinsek, M. Vesenjak, M. Ulbin and Z. Ren, 'Simulation of crash test for high containment level of road safety barriers', *Engineering Failure Analysis*, **14**(2007) 1711-1718.

7. W. Cai and J.Z. Wang, Adaptive multiresolution collocation methods for initial boundary value problems of nonlinear PDEs, *J. Numer. Anal.*, **33**(1996) 937-970.
8. C.F. Chen and C.H. Hsiao, 'Haar wavelet method for solving lumped and distributed–parameter systems', *IEE Proc. Control Theory Appl.*, **144** (1997) 87-94.
9. C.F. Chen and C.H. Hsiao, 'A state-space approach to Walsh series solution of linear systems', *Int. J. System Sci.*, **6** (1965) 833-858.
10. W. Dahmen, A. Kunoth, and K. Urban, A wavelet Galerkin method for the stokes equations, *Computing*, **56** (1996) 259-301.
11. I. Daubechies, 'Orthogonal bases of compactly supported wavelets' *Commun. Pure Appl. Math.*, **41** (1988) 909-996.
12. I. Daubechies, *Ten Lectures on Wavelets*, SIAM, Philadelphia, 1992.
13. U.N. Gandhi and S.J. Hu, 'Data-based approach in modeling automobile crash' *Int. J. Impact Engineering*, **16** (1995) 95-118.
14. A. Graps, An introduction to wavelets, *IEEE Comput. Sci. Eng.* ,**2** (1995) 50-61.
15. M. Griebel, and F. Koster, *Adaptive Wavelet Solvers for the Unsteady Incompressible Navier-Stokes Equations*, Preprint No. 669, Univ. of Bonn, Bonn, Germany, 2000.
16. J. Hallquist and D. Benson, 'DYNA3D–an explicit finite element program for impact calculations. Crashworthiness and Occupant Protection in Transportation Systems', *The Winter Annual Meeting of ASME*, San Francisco, California, 1989.
17. M. Holmstron, Solving hyperbolic PDEs using interpolating wavelets, *J. Sci. Comput.* , **21** (1999) 405-420.
18. B. Jawerth, and W. Sweldens, An overview of wavelet based multiresolution analyses, *SIAM Re.*, **36** (1994) 377-412.
19. M.K. Kaibara, and S.M. Gomes, Fully adaptive multiresolution scheme for shock computations, Goduno methods: Theory and applications, E.F. Toro, ed., Kluwer Academic Plenum Publishers, Manchester, U.K. (2001).
20. M. Kamal, *Analysis and simulation of vehicle to barrier impact*. SAE 700414 (1970).
21. T. Khalil and D. Vander Lugt, 'Identification of vehicle front structure crashworthiness by experiments and finite element analysis. Crashworthiness and occupant protection in transportation systems', *The Winter Annual Meeting of ASME*, San Francisco, California (1989).
22. A. Karami, H.R. Karimi, B. Moshiri, and P.J. Maralani, 'Wavelet-based adaptive collocation method for the resolution of nonlinear PDEs' *Int. J. Wavelets, Multiresoloution and Image Processing*, **5** (2007) 957-973.
23. A. Karami, H.R. Karimi, P.J. Maralani, and B. Moshiri, 'Intelligent optimal control of robotic manipulators using wavelets' *Int. J. Wavelets, Multiresoloution and Image Processing*, **6** (2008) 575-592.
24. H.R. Karimi, B. Lohmann, B. Moshiri, and P.J. Maralani, 'Wavelet-based identification and control design for a class of non-linear systems' *Int. J. Wavelets, Multiresoloution and Image Processing*, **4** (2006) 213-226.
25. H.R. Karimi, 'A computational method to optimal control problem of time-varying state-delayed systems by Haar wavelets', *Int. J. Computer Mathematics*, **83** (2006) 235-246.
26. H.R. Karimi, 'Optimal vibration control of vehicle engine-body system using Haar functions', *Int. J. Control, Automation, and Systems*, **4** (2006) 714-724.
27. H.R. Karimi, and B. Lohmann, 'Haar wavelet-based robust optimal control for vibration reduction of vehicle engine-body system', *Electrical Engineering*, **89** (2007) 469-478.
28. H.R. Karimi, B. Lohmann, P.J. Maralani and B. Moshiri, 'A computational method for parameter estimation of linear systems using Haar wavelets', *Int. J. Computer*

Mathematics, **81** (2004) 1121-1132.
29. H.R. Karimi, P.J. Maralani, B. Moshiri, and B. Lohmann, 'Numerically efficient approximations to the optimal control of linear singularly perturbed systems based on Haar wavelets', *Int. J. Computer Mathematics*, **82** (2005) 495-507.
30. H.R. Karimi, B. Moshiri, B. Lohmann, and P.J. Maralani, 'Haar wavelet-based approach for optimal control of second-order linear systems in time domain', *J. Dynamical and Control Systems*, **11** (2005) 237-252, .
31. H.R. Karimi, M. Zapateiro, and N. Luo, 'Wavelet-based parameter identification of a nonlinear magnetorheological damper' *Int. J. Wavelets, Multiresoloution and Image Processing*, **7** (2009) 183-198.
32. K. Kurimoto, K. Toga, H. Matsumoto and Y. Tsukiji, 'Simulation ofvehicle crashworthiness and its application', *12th Int. Technical Conf. on Experimental Safety Vehicles,* Gotenborg, Sweden (1979).
33. S. Mallat, Multiresolution approximation and wavelet orthogonal bases of $L^2(\mathbb{R})$, *Trans. Amer. Math. Soc.*, **315** (1989) 69-87.
34. D.M. Onchis, and E.M. Suarez Sanchez, The flexible Gabor-wavelet transform for car crash signal analysis, *Int. J. of Wavelets, Multiresolution and Information Processing*, **7** (2009) 481-490.
35. M. Othmani, W. Bellil, C.B. Amar and A.M. Alimi, 'A new structure and training procedure for multi-mother wavelet networks' *Int. J. Wavelets, Multiresoloution and Image Processing*, **8**(1)(2010) 149-175.
36. K.G. Robbersmyr and O.K. Bakken, '*Impact test of Safety barrier, test TB 11'* Project Report 24/2001, ISSN: 0808-5544, 2001.
37. N. Saito, and G. Beylkin, Multiresolution representations using the auto-correlation functions of compactly supported wavelets, *IEEE Trans. Signal Processing* , **41** (1993) 3584-3590.
38. C. Steyer, P. Mack, P. Dubois and R. Renault, 'Mathematical modeling of side collisions.' *12th Int. Technical Conf. on Experimental Safety Vehiles,* vol. 2, Gotenborg, Sweden (1989).
39. J. Walden, Filter bank methods for hyperbolic PDEs, *J. Numer. Anal.* , **36** (1999) 1183-1233.
40. J. Xu, Y. Li, G. Lu and W. Zhou, 'Reconstruction model of vehicle impact speed in pedestrianvehicle accident' *Int. J. Impact Engineering*, **36** (2009) 783-788.